11th International Conference on Marine Technology
MARTEC 2018

Numerical Prediction of Free-Surface Wave around Surface Piercing Marine Rudder

Md. Mashud Karim[1*], Md. Habibur Rahman[1] and Mohammad Salman Yasin[1]

[1]Department of Naval Architecture and Marine Engineering (NAME),
Bangladesh University of Engineering and Technology (BUET), Dhaka – 1000

ABSTRACT

In this research, the effects of free-surface waves and wave induced separation on a 3D surface piercing marine rudder have been studied. The simulation has been performed using a commercial CFD code ANSYS Fluent based on Finite Volume Method (FVM). The predicted results for several Froude numbers (0.19, 0.37, and 0.55) have been studied for surface piercing rudder with NACA 0024 airfoil section and validated with both the experimental data and the previous numerical result. The thickness effects on the wave-induced separation have been evaluated for surface piercing rudder with NACA 0012 and NACA 0018 airfoil sections. It has been found that the wave patterns are dependent on Froude number rather than the thickness of the body at higher Froude number. Free-surface elevations and other flow characteristics have also been evaluated for surface piercing rudder with NACA 0012, NACA 0018, and NACA 0024 airfoil sections.

Keywords: *CFD, marine rudder, Froude number, turbulence, free-surface motion.*

1.0 INTRODUCTION

When a body moves through the free-surface of water, gravity wave is generated around the body due to the pressure variation. Separation of flow occurs at the crest of the wave due to the adverse pressure gradient and extends to the wave trough near the wake of the body. This free-surface wave induced separation is very important in naval architecture, ocean and offshore engineering [1]. Separation due to the free-surface wave deals with the complexities of free-surface deformation, vorticity, turbulence including the 3D boundary layer separation [2].

Chow [3] used surface piercing vertical and submerged horizontal foils to identify the wave induced separation at large depths. He stated that the separation initiated just beyond the wave trough and extended to the following wave crest. Wave induced separation on the boundary layer of a surface-piercing flat plate with an upstream horizontal submerged foil (foil-plate model) was also studied by Stern et al. [4]. Zhang and Stern [5] performed RANS steady-flow simulations with tracking free surface and Baldwin-Lomax turbulence modeling and wave profile experiments for a surface piercing NACA 0024 foil, which has insignificant separation at large depths. They concluded that the flow is naturally unsteady for high Froude numbers and further numerical and experimental study are both required for accurate analysis of flow characteristics and wave breaking. Pogozelski et al. [6] performed an experimental study of the free-surface wave induced separation, but with different foil geometry. Firoozabadi [7] analyzed numerical simulation of free-surface waves and wave induced separation in the presence of an intrusion. Tasif et al. [8] studied the numerical prediction of flow past a 3D rudder with NACA 0012 airfoil section. Karim and Naz [9] investigated the flow field around ship hull including self propulsion characteristics at varying rudder positions using ShipFlow CFD software [10]. Rhee [11] performed numerical simulation of

*Corresponding author: mmkarim@name.buet.ac.bd

free-surface wave flows around surface-piercing cylindrical structures using an unstructured grid-based unsteady Reynolds-averaged Navier–Stokes method.

The previous studies have not yet fully explained the nature of flow on the free-surface with unsteady turbulence model. This paper outlines a numerical procedure to analyze surface piercing rudder with different airfoil sections for explaining the flow features due to free-surface wave and wave induced separation.

2.0 COMPUTATIONAL METHOD

The CFD (Computational Fluid Dynamics) results are obtained by solving RANS equations using the finite volume method. The governing equations, continuity and momentum are, as follows [7]:

$$\frac{\partial U_i}{\partial x_j} = 0, \tag{1}$$

$$\frac{\partial}{\partial x_j}\left(\rho U_i U_j\right) = -\frac{\partial P}{\partial x_j} - \frac{\partial}{\partial x_j}\left(\tau_{ij} + \rho\overline{u_i' u_j'}\right), \tag{2}$$

where $\tau_{ij} = \mu\left(\frac{\partial U_i}{\partial x_j} + \frac{\partial U_j}{\partial x_i}\right)$ is the stress tensor. The treatment for the free-surface flow uses Volume of Fluid (VOF) method [12] for interface tracking. In this method, an additional transport equation is solved for the volume fraction of water in each cell. If the volume fractions of water and air in each cell are denoted as α_w and α_a respectively, the tracking of the interface between the phases is accomplished by the solution of a continuity equation for the volume fraction of water. This equation has the following form:

$$\frac{\partial \alpha_w}{\partial t} + \vec{U}.\nabla\alpha_w = 0, \tag{3}$$

The volume fraction equation will not be solved for air; the volume fraction of air will be computed based on the following constraint:

$$\alpha_w + \alpha_a = 1, \tag{4}$$

The properties appearing in the transport equations are determined by the presence of the component phases in each control volume. For example, the density in each cell is given by the following:

$$\rho = \alpha_w \rho_w + \alpha_a \rho_a, \tag{5}$$

The viscosity is also computed using similar manner.

A single momentum equation is solved throughout the domain and the resulting velocity field is shared among the phases. The momentum equation is dependent on the volume fractions of all phases through the properties, ρ and μ.

The solution is carried out using the Pressure-Implicit with Splitting of Operators (PISO) algorithm. For time discretization, the first order implicit scheme is employed. The Shear-Stress Transport (SST) $k-\omega$ turbulence model is used to capture the boundary layer. This study has been carried out using ANSYS Fluent software, version 18.2, to solve the numerical equations. The grids are generated by this software in order to discretize the physical domain.

3.0 SIMULATION

The effects of free-surface on wave-induced separation of flow past a 3D surface piercing rudder have been studied using a commercial CFD code ANSYS Fluent based on Finite Volume Method. SpaceClaim has been used for model development and ANSYS Workbench for mesh generation. After the mesh generation, the quality of the mesh has been studied.

3.1 TEST CASES

The first test case is surface piercing rudder with NACA 0024 airfoil section, with 1.0m chord length, *L*, and 1.0m span (50% in water). A structured mesh is adopted for the domain. The simulation has been done for three Froude numbers (Fr = 0.19, 0.37, and 0.55). Only half of the domain is solved, since the geometry is symmetry, with 325500 hexahedral structured cells. Fine grids are used near the body and the free-surface whereas the rest of the domain is coarse.

The second test case is surface piercing rudder with NACA 0012 airfoil section, with a chord length of 1.0m, a span of 1m (50% in water) and 325500 hexahedral cells. A structured mesh is used for the domain. Like NACA 0024 foil, fine grid is used near the body and the free-surface, and coarse grid is used in the rest of the domain.

The third test case is surface piercing rudder with NACA 0018 airfoil section. It consists of 1.0m chord length and 1.0m span (50% in water). The domain is structured with 325500 hexahedral cells. Fine grid is adopted near the body and the free-surface. Second and third cases are used to evaluate the thickness effects on the free-surface wave and wave induced separation.

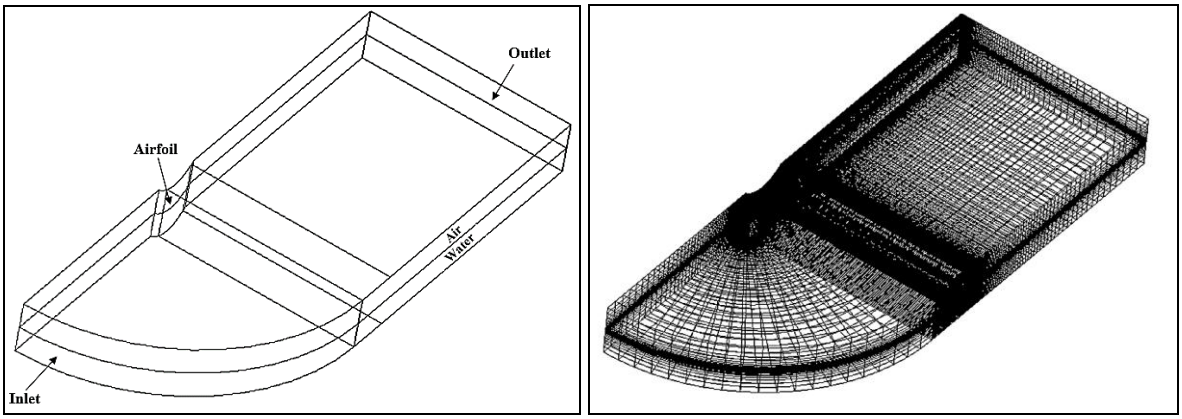

(a) (b)

Figure 1: (a) Geometry (b) computational grid for rudder.

Figure 1 (a) and (b) show the geometry and structured grid for a rudder respectively. The domain and boundaries are shown in figure 1 (a). As for boundary condition, upstream is modeled as "Pressure Inlet", the downstream as "Pressure Outlet". "No Slip" condition is used for the surface of the foil. Top, bottom and the sides are defined as "Symmetry".

3.2 GRID STUDY

After grid generation, grid independency test has been carried out and after completion of the test, we get the quality report as:

Table 1: Quality report of 3D surface piercing rudder with different airfoil sections.

Mesh Quality	NACA 0012	NACA 0018	NACA 0024
Minimum orthogonal quality	0.00124	0.00124	0.00142
Maximum orthogonal skew	0.2997	0.2664	0.2142
Maximum aspect ratio	106.39	106.39	106.39

In the above quality report, it has been shown that the produced grid for 3D rudder with NACA 0012, NACA 0018 and NACA 0024 airfoil sections are fine enough to perform the simulation.

4.0 RESULT AND DISCUSSION

Figure 2 (a) shows the wave profile along rudder with NACA 0024 airfoil section for Fr = 0.19 which agrees well with Zhang and Stern experimental data and Firoozabadi numerical result. The wave pattern in this case is nearly as much similar to the experimental and numerical results showing that the effect of air is negligible. The wavelength is slightly greater than the Kelvin wave length ($\lambda = 2\pi Fr^2$). The wave pattern is flat in the separation region from x/L = 0.40 to x/L = 1.00. The bow wave peak is at about 2% of chord length, L.

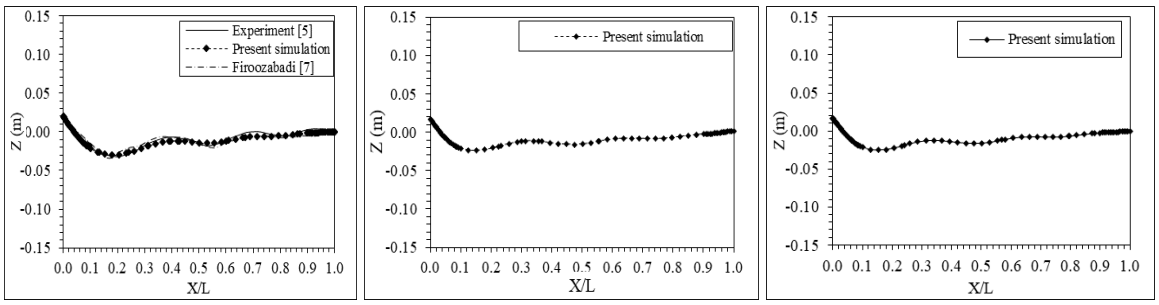

(a) (b) (c)

Figure 2: Wave profile for Fr = 0.19 along rudder with (a) NACA 0024 (b) NACA 0012 and (c) NACA 0018 foil sections.

Figure 2 (b) and (c) represent the wave profile along rudder with NACA 0012 and NACA 0018 airfoil sections for Fr = 0.19. The wave pattern shows no significant change due to the thickness effect. The wave height, wave steepness, and the distortion in the separation region are dependent on Fr, but not on thickness. The wave patterns for NACA 0012 and NACA 0018 are flat in the region from x/L = 0.30 to x/L = 1.00 and x/L = 0.35 to x/L = 1.00 respectively and the bow wave peaks are both at about 1.7% of L.

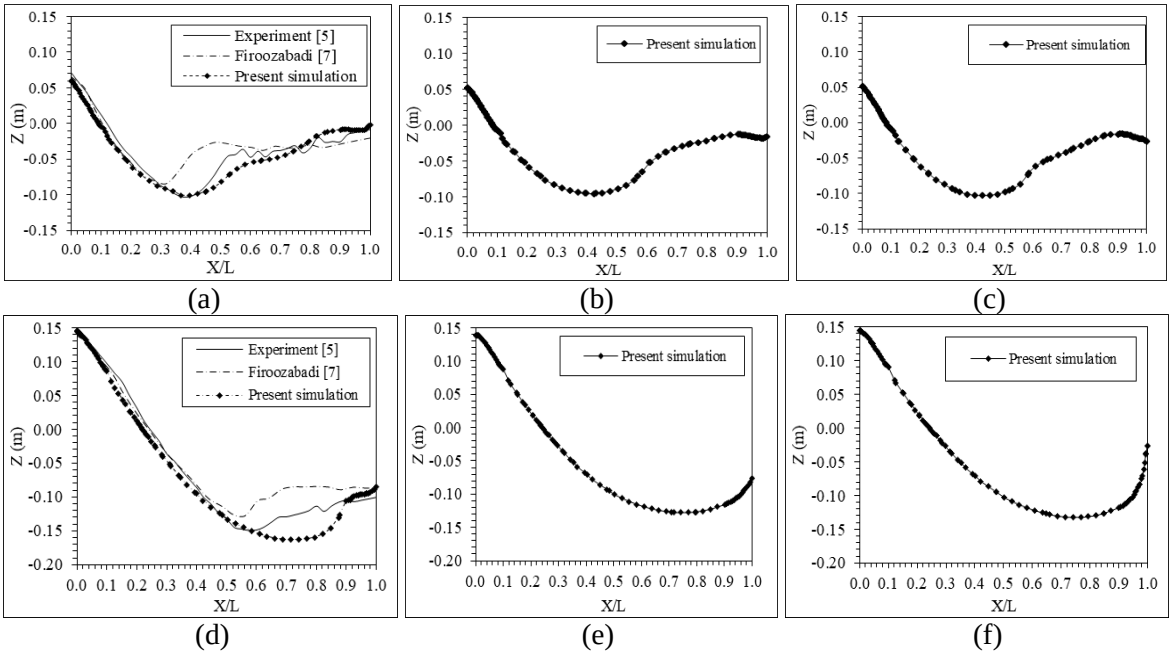

(a) (b) (c)

(d) (e) (f)

Figure 3: Wave profile for Fr = 0.37 along rudder with (a) NACA 0024 (b) NACA 0012 (c) NACA 0018 foil section, and for 0.55 along (d) NACA 0024 (e) NACA 0012 (f) NACA 0018 foil sections.

Figure 3 (a) and (d) show the wave profile along rudder with NACA 0024 airfoil section for Fr = 0.37 and Fr = 0.55 respectively. The results agree with the experimental results. The wave steepness and wave height are larger at Fr = 0.55 than those at Fr = 0.19 due to higher pressure at stagnation point and the air effects dominate the flow. The bow wave peak for Fr = 0.37 and Fr = 0.55 are at about 6% and 14.5% of chord length, *L* respectively. The wave pattern is flat in the separation region for Fr = 0.37, but for Fr = 0.55 the wave steepness increases and the flat pattern decreases.

Figure 3 (b), (c), (e) and (f) represent the wave profile for Fr = 0.37 and Fr = 0.55 along rudder with NACA 0012 and NACA 0018 airfoil sections. The free-surface elevation is greater at Fr = 0.55 than that at Fr = 0.19. The wave patterns, i.e., the wave steepness, wave height, and the distortion in the separation region, increase with the increase in Froude number and the effects of air become significant.

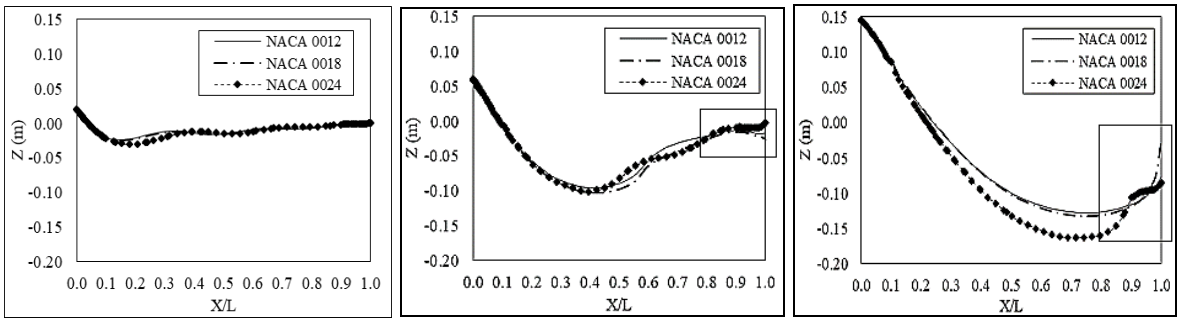

(a) (b) (c)

Figure 4: Comparison of the wave profile along different rudder sections at (a) Fr = 0.19 (b) Fr = 0.37 and (c) Fr = 0.55.

Figure 4 shows the comparison of the wave profile along rudder with different airfoil sections for different Froude numbers. For Fr = 0.19, the free-surface elevation is small and agrees with the experimental results. The air effects are negligible for low Froude number. With the increase in Froude number, the free-surface elevation increases with a constant steepness and the air effects dominate the flow. The wave pattern also increases and it becomes more complicated for Fr = 0.55. The wave height is negative in the wake section and also behind the separation region for Fr = 0.37 and Fr = 0.55. The wave height and the distortion in the separation region are greater for Fr = 0.55 than for Fr = 0.19 and Fr = 0.37. For Fr = 0.55, although the primary pattern of the wave is dependent on Froude number, the thickness effects dominate the flow. The wave pattern in the separation region is pretty much similar for NACA 0012 and NACA 0018 airfoil sections but changes for NACA 0024 with the increase in thickness.

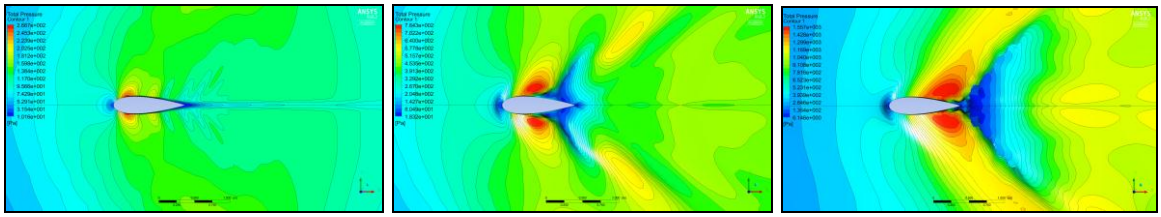

(a) (b) (c)

Figure 5: Pressure contours for rudder with NACA 0024 airfoil section at (a) Fr = 0.19 (b) Fr = 0.37 and (c) Fr = 0.55.

Figure 5 represents the contour of pressure for rudder with NACA 0024 airfoil section at different Froude numbers. For Fr = 0.19, the maximum pressure occurs in the region from *x/L* =

0.14 to *x/L* = 0.23. The waves are found to be insignificant far from the body. The boundary layer is too small for low Froude numbers. The pressure gradients become steeper for higher Fr numbers and extend beyond the body. At Fr = 0.37 and Fr = 0.55, the maximum pressure occurs from *x/L* = 0.35 to *x/L* = 0.56 and from *x/L* = 0.61 to *x/L* = 0.99 respectively.

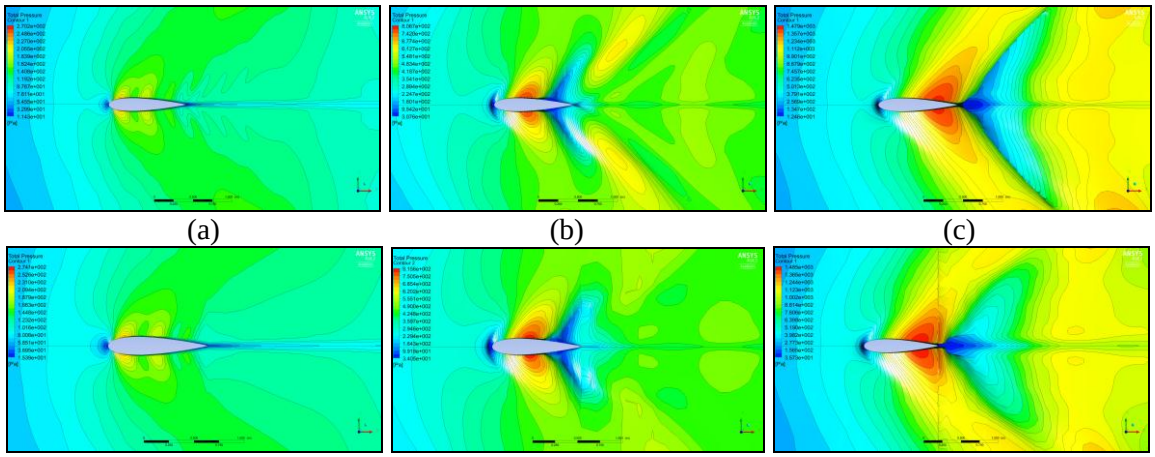

(a) (b) (c)

(c) (d) (e)

Figure 6: Pressure contours for rudder with NACA 0012 at (a) Fr = 0.19 (b) Fr = 0.37 (c) Fr = 0.55 and for NACA 0018 at (d) Fr = 0.19 (e) Fr = 0.37 and (f) Fr = 0.55.

Figure 6 represents the pressure contours for 3D surface piercing rudder with NACA 0012 and NACA 0018 airfoil sections at different Froude numbers. The separation region of water extends with the increase in Fr number. Figure shows that at low Froude number the separation is insignificant, but high at larger Froude number. The wave deformation depends on the thickness but not on Fr at lower Froude number, but it depends on Fr instead of thickness at higher Froude number.

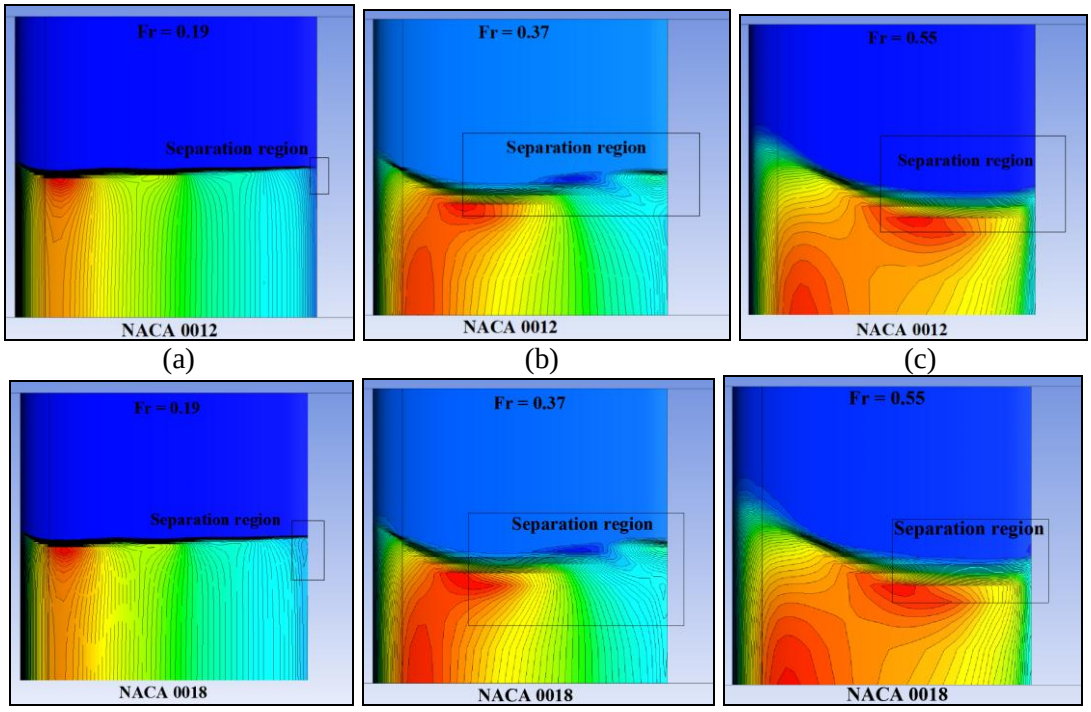

(a) (b) (c)

(d) (e) (f)

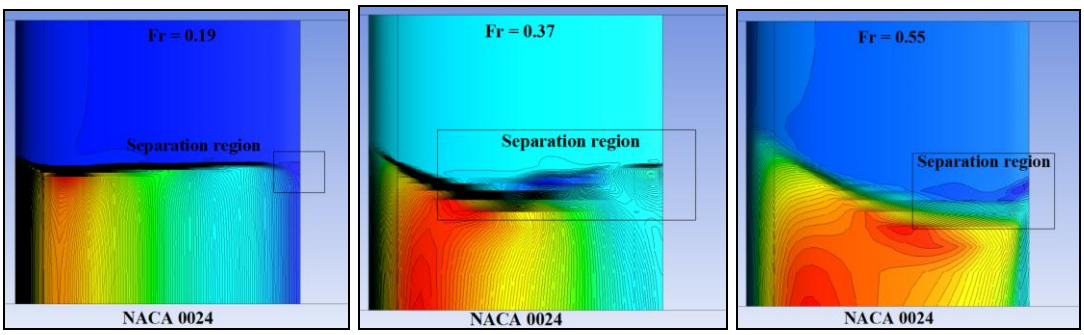

(g) (h) (i)

Figure 7: X-wall shear stress contours for rudder with NACA 0012 section at (a) Fr = 0.19 (b) Fr = 0.37 (c) Fr = 0.55; with NACA 0018 section at (d) Fr = 0.19 (e) Fr = 0.37 and (f) Fr = 0.55; and with NACA 0024 at (g) Fr = 0.19 (h) Fr = 0.37 and (i) Fr = 0.55.

Figure 7 represents the X-wall shear stress contours for rudder with different airfoil sections at different Froude numbers. The separation regions are also marked where the shear stress values are negative. For Fr = 0.19, the separation region is very small and the wave effects are insignificant. But with the increase in Froude number, the wave effects dominate the flow pattern and the separation zone extends. Thus the X-wall shear stress is pretty much similar regardless of the thickness and dependent on Fr at higher Froude numbers.

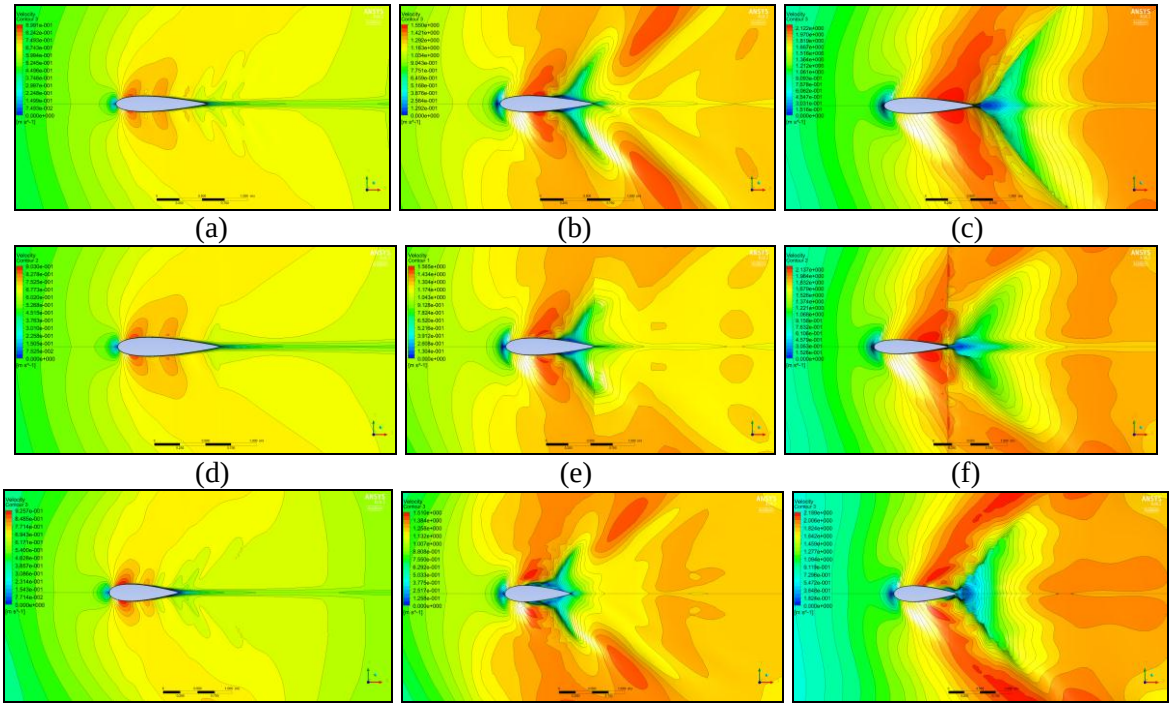

(a) (b) (c)

(d) (e) (f)

(d) (e) (f)

Figure 8: Wave Patterns for rudder with NACA 0012 section at (a) Fr = 0.19 (b) Fr = 0.37 (c) Fr = 0.55; with NACA 0018 section at (d) Fr = 0.19 (e) Fr = 0.37 and (f) Fr = 0.55; and with NACA 0027 section at (g) Fr = 0.19 (h) Fr = 0.37 and (i) Fr = 0.55.

Figure 8 represents the wave pattern for 3D rudder with NACA 0012, NACA 0018, and NACA 0024 airfoil sections at different Froude numbers. For Fr = 0.19, the wave pattern is similar for all airfoil sections. For higher Froude number, the wave pattern is dependent on Fr but not on

thickness which suggests that the profile is same in every case and the gravity effect dominates the pattern. The pressure distribution is limited to the free-surface only. The thickness effect is noticeable in the bow wave peak, extent of the free-surface, at the wake region, and also in the separation region.

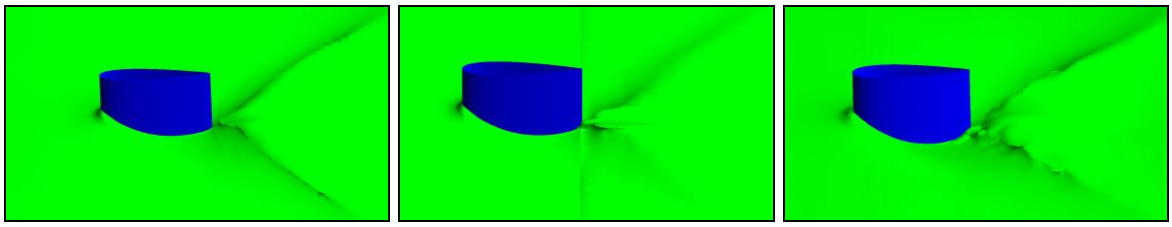

(a) (b) (c)

Figure 9: 3D view of free-surface for rudder with (a) NACA 0012 (b) NACA 0018 and (c) NACA 0018 airfoil sections.

Figure 9 shows the 3D views of the free-surface for surface piercing rudder with NACA 0012, NACA 0018, and NACA 0024 airfoil sections at Fr = 0.55. The bow wave peak increases with the increase in thickness. The separation around the body, free-surface elevation, wave height, and the wave steepness is discernible in the figure.

5.0 CONCLUSIONS

Finite Volume Method (FVM) has been successfully applied to study the effects of free-surface on wave-induced separation of flow past a 3D marine rudder. The computed results agree with both the available experimental data and the previous numerical result. The thickness effects have been successfully investigated using surface piercing rudder with NACA 0012 and NACA 0018 airfoil sections. The Shear-Stress Transport (SST) k-ω turbulence model captured the boundary layer well and the Volume of Fluid (VOF) technique successfully tracked the free-surface. The results are same in all cases except some changes at higher Froude number (Fr) due to the larger thickness. The study indicates that the wave patterns, i.e., the wave height, wave steepness, the distortion in the separation region, and the free-surface elevations, become more significant with the increase in Froude number. The bow wave peak increases at higher value of Fr. For very high value of Fr, the flow becomes highly unsteady and the separation region extends. The air effects dominate the flow at medium (Fr = 0.37) and higher Froude number (Fr = 0.55). However, the results may be limited due to the mesh quality and the computational method. Further study can be performed to analyze the shape effects on the free-surface wave-induced separation. Other turbulence models can be used to study the free-surface waves and wave induced separation and to evaluate the performance.

ACKNOWLEDGEMENTS

Authors are grateful to Bangladesh University of Engineering and Technology (BUET) and sub-project CP # 2084 of Department of Naval Architecture and Marine Engineering under Higher Education Quality Enhancement Project (HEQEP), UGC, Ministry of Education, Govt. of Bangladesh for providing necessary research facilities during the current research work.

REFERENCES

1. Iafrati, A., 2017. Flow around ships and underwater vehicles, *Encyclopedia of Maritime and Offshore Engineering*, Vol. 01, pp 169-180.
2. Adjali, S., Belkadi, M., Aounallah, M. and Imine, O., 2015. A numerical study of steady 2D flow around NACA 0015 and NACA 0012 hydrofoil with free surface using VOF method, *EPJ Web of Conference*, 92, 02001.
3. Chow, S.K., 1967. *Free-surface effects on boundary-layer separation on vertical struts*, PhD Thesis, University of Iowa, USA.
4. Stern, F., Hwang, W.S. and Jaw, S.Y., 1989. Effects of waves on the boundary layer of a surface-piercing flat plate: experiment and theory, *Journal of Ship Research*, Vol. 33, pp 63-80.
5. Zhang, Z. and Stern, F., 1996. Free-surface wave-induced separation, *Journal of Fluid Engineering*, Vol. 118, pp 546-554.
6. Pogozelski, E., Katz, J. and Huang, T., 1997. The flow structure around a surface-piercing strut, *Physics of Fluids*, Vol. 9 (5), pp 1387-1399.
7. Sadathosseini, S.H., Mousaviraad, S.M., Firoozabadi, B. and Ahmadi, G., 2008. Numerical simulation of free-surface waves and wave induced separation, *Science Iranica*, Vol. 15, No. 3, pp 232-331.
8. Tasif, T.H., Fazle, A.B. and Rahman, M.H., 2016. *Computational study of flow past 3D rudder with NACA 0012 airfoil*, B.Sc. Engg. Thesis, Dept. of NAME, BUET, Bangladesh.
9. Karim, M. M. and Naz, N., 2016. Computation of flow field around ship hulls including self propulsion characteristics of propeller at varying rudder positions, *Procedia Engineering, Elsevier*, Vol. 194, pp 96-103.
10. Nabila, N., 2017. *Numerical simulation of flow around ship hull considering rudder-propeller interaction*, M.Sc. Engg. Thesis, Dept. of NAME, BUET, Bangladesh.
11. Rhee, S.H., 2009. Unsteady Reynolds averaged Navier–Stokes method for free-surface wave flows around surface-piercing cylindrical structures, *Journal of Waterway, Port, Coastal, and Ocean Engineering*, Vol. 135, pp 135-143.
12. Karim, M. M., Prasad, B. and Rahman, N., 2014. Numerical simulation of free surface water wave for the flow around NACA 0015 hydrofoil using the volume of fluid (VOF) method, *Ocean Engineering, Elsevier*, Vol. 78, pp 89-94.